Journal of Materials Chemistry C

Accepted Manuscript

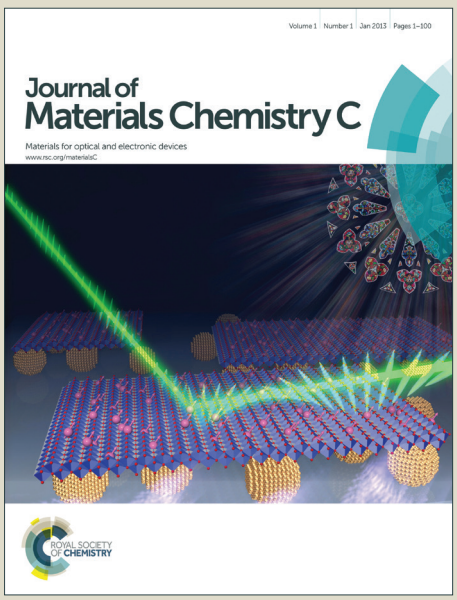

ROYAL SOCIETY OF CHEMISTRY

www.rsc.org/materialsC

Thermal Stable Luminescence and Structure Evolution of $(K,Rb)BaPO_4:Eu^{2+}$ Solid-Solution Phosphors

Chenglong Zhao[1], Zhiguo Xia[2*], Shixin Yu[1]

[1]*School of Materials Sciences and Technology, China University of Geosciences, Beijing 100083, China*

[2]*School of Materials Sciences and Engineering, University of Science and Technology Beijing, Beijing 100083, China*

---

[*] **Corresponding author:**

Zhiguo Xia

E-mail: **xiazg@ustb.edu.cn**

School of Materials Sciences and Engineering, University of Science and Technology Beijing, Beijing 100083, China

Tel. : +86-10-8237-7955;

Fax. : +86-10-8237-7955

†Electronic supplementary information (ESI) available. See DOI:xxx

Abstract: The orthophosphate phosphors $ABaPO_4:Eu^{2+}$ (A = K, Rb) have been studied in this paper. The continuous solid-solution phases among $(K_x,Rb_{1-x})BaPO_4$ have been determined and the phase structure evolution has been discussed depending on K/Rb ratio, and all the Eu^{2+}-doped $(K_x,Rb_{1-x})BaPO_4$ phosphors show blue emission peaking at near 420 nm originating from 4f-5d transition of Eu^{2+}. The difference of the fine microstructure has been investigated and the effect on the photoluminescence behaviors, especially the thermal stable luminescence has been studied for this series of solid-solution phosphors. The relationship between activation energy and thermal stable luminescence is also discussed. The composition optimized $(K_x,Rb_{1-x})BaPO_4:Eu^{2+}$ phosphor can be potential in the application of the phosphor-converted white light-emitting diodes (*w*-LEDs).

1. Introduction

The research history of orthophosphate compounds with the general formula $ABPO_4$ (where A is monovalent cation and B is divalent cation.) can date back to the 1962.[1-2] This large family of $ABPO_4$ compounds with various crystal structure types can demonstrate low sintering temperature, high thermal and chemical stability.[3-7] Recently, $ABPO_4$ compounds have been extensively reported as a kind of suitable phosphors hosts, and different rare earth ions can be introduced into the A or B cationic sites showing multi-color emission.[8-11] It is also believed that the different kinds of sites (A or B ions) will possibly induce the formation of various crystal structures or different crystal field environment when they are occupied by the rare earth ions. That's to say, various crystal structure of orthophosphate phosphors provide many appropriate hosts for activators ions to regulate characteristic properties.[12-13]

Herein, $KBaPO_4$ and $RbBaPO_4$ possess the same crystal structure[14], and so far $KBaPO_4:Eu^{2+}$ and $RbBaPO_4:Eu^{2+}$ have been also reported by W. B. Im *et al* [15] and H. J. Song *et al* [16], respectively. However, the difference of the fine crystal structure and the luminescence properties, as well as the effect on the thermal stability for the two types of orthophosphates and $(K,Rb)BaPO_4:Eu^{2+}$ solid-solution phosphor is unclear. In this work, we have fabricated $KBaPO_4:Eu^{2+}$, $RbBaPO_4:Eu^{2+}$ and $(K,Rb)BaPO_4:Eu^{2+}$, phosphors and the detailed crystal structure information were comparatively investigated. Correlation of the crystal structure and luminescence properties for this series of orthophosphate phosphors have been discussed and established, which will

help to the understanding of the "structure-property" of the rare earth luminescence materials. It is further believed that the composition optimized $(K_x,Rb_{1-x})BaPO_4:Eu^{2+}$ phosphor can be potential as the blue-emitting component in white light-emitting diodes (*w*-LEDs).

2. Experimental Section

Phosphate phosphors of $ABaPO_4:Eu^{2+}$ (A = K, Rb) were synthesized by a traditional high temperature solid-state reaction. The stoichiometric amounts of K_2CO_3 (A.R.), Rb_2CO_3 (A.R.), $BaCO_3$ (A.R.), $(NH_4)_2HPO_4$ (A.R.) and Eu_2O_3 (99.99%) were intimately mixed homogeneously and pre-heated at 500 ^oC for 3h in air atmosphere in alumina crucibles with covers. After cooling to room temperature, the preliminary products were ground thoroughly in an agate mortar and then were placed into alumina crucibles and annealed at 1200 ℃ in a CO reducing atmosphere for 4 h with highly pure carbon particles as a reducing agent. Finally, the samples were, after cooling to room temperature in the furnace, ground to fine powders for properties characterization.

The phase purity of phosphate phosphors $ABaPO_4:Eu^{2+}$ (A = K, Rb) samples were measured by the X-ray diffractometer (XRD-6000, SHIMADZU, China) with Cu-Kα radiation (λ = 0.15406 nm), operating at 40 kV, 30 mA. The continuous scanning rate (2θ ranging from 10^o to 70^o) used as phase formation determination was 4^o (2θ)/min and step scanning rate (2θ ranging from 5^o to 120^o) used for Rietveld analysis was 8 s/step with a step size of 0.02. Powder diffraction data were obtained

using a computer software General Structure Analysis System (GSAS) program. The photoluminescence (PL) spectra and excitation (PLE) spectra were recorded using a fluorescent spectrophotometer (F-4600, HITACHI, Japan) with a photomultiplier tube operating at 400V, and a 150W Xe lamp at room temperature, the temperature-dependence luminescence properties were measured on the same spectrophotometer combined with a self-made heating attachment and a computer-controlled electric furnace. The room temperature decay curves and time resolved PL spectra were recorded on a JOBIN YVON FL3-21 spectro-fluorometer and the 370 nm pulse laser radiation (nano-LED).

3. Results and Discussion

3.1 Phase structure

As mentioned above $KBaPO_4$ and $RbBaPO_4$ belong to the iso-structural compounds. Then, $(K_x,Rb_{1-x})Ba_{0.97}PO_4:0.03Eu^{2+}$ (x = 0-1) were synthesized to explore the K/Rb ratio dependent phase structure evolution and luminescence properties. On the basis of the luminescence properties' investigation, $K_{0.2}Rb_{0.8}Ba_{0.97}PO_4:0.03Eu^{2+}$ was found to show the strongest emission intensity among this series of samples, so the sample with this composition was selected as the following structure study. **Fig. 1** shows the selected powder XRD patterns of as-prepared $RbBa_{0.97}PO_4:0.03Eu^{2+}$, $K_{0.2}Rb_{0.8}Ba_{0.97}PO_4:0.03Eu^{2+}$ and $KBa_{0.97}PO_4:0.03Eu^{2+}$, respectively, and the standard patterns of $RbBaPO_4$ phase (JCPDS-81-647) and $KBaPO_4$ phase (JCPDS-84-1462) are also given as a comparison.[17] We found that the XRD patterns of the two end

members ($RbBa_{0.97}PO_4$:$0.03Eu^{2+}$ and $KBa_{0.97}PO_4$:$0.03Eu^{2+}$) are consistent with the corresponding standard data, and XRD pattern $K_{0.2}Rb_{0.8}Ba_{0.97}PO_4$:$0.03Eu^{2+}$ seems to be consistent with either of them. In order to further understand the microstructure difference among them, the detailed Rietveld refinement was performed for the samples.[18-19] **Fig. 2** provides the results of the experimental and the calculated powder XRD for three compounds. **Fig. 2 a)** and **b)** gave the Rietveld refinement results for the two end members, which showed that there were no impurity peaks detected for the as-prepared $KBaPO_4$:$0.03Eu^{2+}$ and $RbBaPO_4$:$0.03Eu^{2+}$ samples. When we try to fit the XRD pattern of the $K_{0.2}Rb_{0.8}BaPO_4$:$0.03Eu^{2+}$ phase, the two initial models corresponding to $KBaPO_4$ phase (ICSD-202430) and $RbBaPO_4$ phase (ICSD-672001) are both tried to refine. As shown in **Fig. 2 c)** and **d)**, we got the acceptable results for both of them**.** **Table 1** presents the main crystallographic parameters for $KBaPO_4$:$0.03Eu^{2+}$, $RbBaPO_4$:$0.03Eu^{2+}$ and $K_{0.2}Rb_{0.8}BaPO_4$:$0.03Eu^{2+}$ samples, and the results confirms that $K_{0.2}Rb_{0.8}BaPO_4$ is indeed iso-structural to $KBaPO_4$ and $RbBaPO_4$. As the same time, it indicates that these three compounds share the same crystalline orthorhombic crystal system with a space group *Pnma* (62), and we can find that the cell parameters become bigger from $KBaPO_4$:$0.03Eu^{2+}$ to $K_{0.2}Rb_{0.8}BaPO_4$:$0.03Eu^{2+}$, and finally to $RbBaPO_4$:$0.03Eu^{2+}$, and it is ascribed to the fact that the ion radii of Rb^+ ($R_{CN=8}$=1.66Å) is bigger than that of K^+ ($R_{CN=8}$=1.52Å). As a further examination of the utility of the K^+ and Rb^+ substitutions, the unit cell parameters (*a*, *b*, *c* and *V*) of $K_xRb_{1-x}Ba_{0.97}PO_4$:$0.03Eu^{2+}$ solid-solution series obtained from Rietveld analysis are given in **Fig. 3**, we can see the lattice constants *a*, *b*, *c* and unit cell volume *V* are

proportional to the *x* value. According to the Vegard's law, the crystal lattice parameter of an alloy and cell volume change with the concentrations of the constituent elements.[20] The linear evolution of the cell parameters in **Fig. 3** illustrated that this series of $K_xRb_{1-x}Ba_{0.97}PO_4:0.03Eu^{2+}$ compounds belong to the continuous iso-structural solid-solution.

3.2 Luminescence Properties

The representative photoluminescence excitation (PLE) and photoluminescence excitation (PL) spectra of as-prepared $K_{0.2}Rb_{0.8}Ba_{0.97}PO_4:0.03Eu^{2+}$ phosphor were shown in Fig. 4. The excitation spectrum ranging from 200 to 400 nm is composed of one strong absorption peak at 245 nm and two weak absorption peaks located around 300 and 337 nm, which is attributed to $4f^7(^8S_{7/2})$-$4f^6 5d$ transitions of the doped Eu^{2+} ions. Under the excitation at 325 nm, the phosphor exhibited a blue emission band peaked at 424 nm. **Fig. 5** shows the PL spectra of $K_xRb_{1-x}Ba_{1-0.97}PO_4:0.03Eu^{2+}$ (x=0-1) solid-solution phosphors, which exhibit the intense blue-emitting color with emission peak in the range of 410–430 nm, which is assigned to the transitions between the ground state $4f^7$ and the crystal-field split $4f^6 5d$ configuration. As shown in **Fig. 5**, the emission intensities increased with increasing x values (Rb content), and maximized at x = 0.2, and then decreased with Rb content. As for the variation of the emission peaks' positions of $K_xRb_{1-x}Ba_{1-0.97}PO_4:0.03Eu^{2+}$, it is found that the red-shift can be clearly found, as show in the arrow in the figure. For the purpose of determining the emission position of the Eu^{2+} ion, it is strongly dependent on its surrounding environment, and the following experiential equation reported by Van Uitert is

employed to explain this phenomenon.[21]

$$E = Q\left[1 - \left(\frac{V}{4}\right)^{\frac{1}{V}} 10^{-\frac{n \times E_a \times r}{80}}\right] \quad (1)$$

where E is the energy position for the rare-earth ion emission peak (cm^{-1}), here is equivalent to the wavelength of 417-426 nm, Q is the position in energy for the lower d-band edge for the free ion (34,000 cm^{-1} for Eu^{2+}), V is the valence of the "active'' cation, here V = 2 for Eu^{2+}. Ea is the electron affinity of the atoms that form anions. Here, E_a is approximately determined as approximate 2.19 eV, as reported in other samples.[22] n is the number of anions in the immediate shell around the ''active'' cation, and r is the radius of the host cation (Ba^{2+}) replaced by the ''active'' cation (Eu^{2+}). It can be calculated that the d-band edge in energy E is 23, 676 cm^{-1} equivalent with approximate energy value in the wavelength range of 417-426 nm, the result demonstrates that Eu^{2+} center that shows blue luminescence should come from nine-coordination Eu^{2+} site.

The PL spectra of the $KBa_{1-x}PO_4:xEu^{2+}$, $RbBa_{1-x}PO_4:xEu^{2+}$, $K_{0.2}Rb_{0.8}Ba_{1-x}PO_4:xEu^{2+}$ phosphors with various Eu^{2+} activator concentrations were shown in **Fig. S1**. All the broad emission bands are due to the transition from the ground state $4f^7$ to the excited state $4f^65d$ of Eu^{2+}. Since the 5d state is easily influenced by the crystal field, different crystal fields can split the 5d state in different ways, which in turn induce the variation of the emission band.[23-24] It is also found from **Fig. S1** that the optimum Eu^{2+} content is determined to be 3 mol% owing to the concentration quenching effect, which is ascribed to the energy transfer between Eu^{2+} ions and the other ions or the energy transfer to traps or quenching sites. In order to

explain the concentration quenching phenomena of these samples, the crystal distance R_c between the Eu^{2+} ions can be calculated by using concentration quench method proposed by Blasse.[25-26]

$$R_C \approx 2\left(\frac{3V}{4\pi x_c N}\right)^{\frac{1}{3}} \quad (2)$$

where V is the volume of the unit cell, N is the number of host cations in the unit cell, x_c is the concentration of Eu^{2+} ion. In this work, $KBa_{0.97}PO_4$:$0.03Eu^{2+}$, $RbBa_{0.97}PO_4$:$0.03Eu^{2+}$ and $K_{0.2}Rb_{0.8}Ba_{0.97}PO_4$:$0.03Eu^{2+}$ these three compounds N = 4, V = 435.107 $Å^3$, 448.862 $Å^3$ and 440.442 $Å^3$, X_c is 0.03 for emission peak at 417 nm, 426 nm and 424 nm, respectively. According to this equation, *Rc* is determined to be 18.80 Å, 18.93 Å and 18.89 Å, respectively. Moreover, the red-shift of the peak wavelength can be clearly observed with increasing Eu^{2+} concentration, as shown in **Fig. 6**. Therefore, the equation (3) is employed to elucidate the *d*-orbital splitting of the metal center and the induced red-shift.[27]

$$D_q = \frac{ze^2r^4}{6R^5} \quad (3)$$

Where *Dq* is the energy level separation, *z* is the charge or valence of the anion ligand, *e* is the charge of an electron, and *r* is the radius of the *d* wave function, *R* is the distance between the central ion and its ligands. In this work, the *R* is the distance between the Eu^{2+} ion and its ligands O^{2-} ions, and we have obtained this distance for these three compound from the result of Rietveld refinement. It is found that *R* values are 2.841(3) Å, 2.848(0) Å and 2.854(6) Å for $KBaPO_4$:$0.03Eu^{2+}$, $RbBaPO_4$:$0.03Eu^{2+}$ and $K_{0.2}Rb_{0.8}BaPO_4$:$0.03Eu^{2+}$ samples, respectively. For $d_{(Eu\text{-}O)}$-orbital, *z*, *e* and *r* are equal, then *Dq* is only the function of $1/R^5$, so the smaller *R* is, the bigger *Dq* is, then

the much bigger the electrostatic interaction is, which can cause crystal field to split easily resulting in the red shift of emission wavelengths. Except for this, the red-shift of emission peak can be found in many Eu^{2+}-doped phosphors with increasing concentration due to the variations of crystal field strength surrounding the activators. As can be seen in Fig. 6, the emission peaks of the samples shifted to the long wavelength region with increasing Eu^{2+} concentration. It is accepted that the inter-atomic distance between the two activators become shorter, and the interaction is enhanced. Thus the crystal field strength surrounding Eu^{2+} is increased, and results in the red-shift of the emission peak. However, the position of the emission peak for $KBa_{1-x}PO_4:xEu^{2+}$ is shorter than that of $K_{0.2}Rb_{0.8}Ba_{1-x}PO_4:xEu^{2+}$, but the emission wavelength of $RbBa_{1-x}PO_4:xEu^{2+}$ disagrees with this discipline, which illustrates electrostatic interaction is not the unique factor influencing in the red shift phenomenon. We know that the surrounding environment of Eu^{2+} is partly ascribed to the difference of the chemical composition, crystal structure and possible structural variation (change of the bond length or angle) or defect. Therefore, many factors can induce the observed shift of the emission peaks, as we discussed above. [28-30]

3.3 Thermal stable luminesence, lifetime and CIE values

Fig. 7 shows the temperature dependence of the PL spectra of $KBa_{0.97}PO_4:0.03Eu^{2+}$, $RbBa_{0.97}PO_4:0.03Eu^{2+}$ and $K_{0.2}Rb_{0.8}Ba_{0.97}PO_4:0.03Eu^{2+}$ monitored by 325 nm. It is found that $KBa_{0.97}PO_4:0.03Eu^{2+}$ has relatively poor thermal stability; however, the other two compositions show better thermal stability. In order to give a quantitative analysis on the thermal stable luminescence behaviors, the Arrhenius equation was employed to calculate the respective activation energy as following: [31]

$$I_T = \frac{I_0}{1+c\exp(-\frac{\Delta E}{kT})} \quad (4)$$

where I_0 is the initial PL intensity of the phosphor at 25 ℃, I_T is the intensity at a given temperature T, c is a constant, E is the activation energy for thermal quenching, and k is the Boltzmann constant (8.617×10^{-5} eV k^{-1}). Based on the equation, the activation energy ΔE can be calculated via a linear fitting of $\ln[(I_0/I)-1]$ against $1/kT$, where a straight slope equals $-\Delta E$. As shown in **Fig. 8**, ΔE was intended to be 0.137 eV, 0.279 eV and 0.319 eV for $KBa_{0.97}PO_4:0.03Eu^{2+}$, $RbBa_{0.97}PO_4:0.03Eu^{2+}$ and $K_{0.2}Rb_{0.8}Ba_{0.97}PO_4:0.03Eu^{2+}$, respectively. It is very interesting to find that the activation energy values are consistent with the evaluation of the thermal stability. As shown in **Fig. 7**, the emision intensities decreased to 71.26%, 91.65% and 93.68% at 503 K for $KBa_{0.97}PO_4:0.03Eu^{2+}$, $RbBa_{0.97}PO_4:0.03Eu^{2+}$ and $K_{0.2}Rb_{0.8}Ba_{0.97}PO_4:0.03Eu^{2+}$ suggesting that $RbBa_{0.97}PO_4:0.03Eu^{2+}$ and $K_{0.2}Rb_{0.8}Ba_{0.97}PO_4:0.03Eu^{2+}$ have the better thermal stabilities, but $KBa_{0.97}PO_4:0.03Eu^{2+}$ is inferior to the others. Here we proposed to build up the relationship between the practical thermal stabilities and the calculated activation energy ΔE. It is accepted that the factors influencing in spectral intensity are as follows, a) The energy difference between the high energy level E_j and the low-lying level E_i,; b) The number of excitation electron n_j in the high energy level; c) The frequency of the transition from excitation-emission A_{ij}.

At the thermodynamic equilibrium state, the number of electrons in different energy levels follows the Boltzmann distribution law, so the concentration of electron in the high energy level E_j and the low-lying level E_i are n_j and n_i, respectively.

$$n_j = n_i \frac{g_j}{g_i} e^{-\frac{E_j - E_i}{kT}} \quad (5)$$

where $g = 2J + 1$, g is statistical-weight factor, J is quantum numbers, k is the Boltzmann constant. If the low-lying level is the ground state, E_i is 0.

$$n_j = n_0 \frac{g_j}{g_0} e^{-\frac{E_j}{kT}} \quad (6)$$

The equation of emission intensity is

$$I_j = A_{0j} h\nu n_j = A_{0j} h\nu n_0 \frac{g_j}{g_0} e^{-\frac{E_j}{kT}} \quad (7)$$

The damping of emission intensity can be expressed by the below equation (where $I_m > I_n$):

$$\frac{I_m}{I_n} = \frac{A_{0m} g_m}{A_{0n} g_n} e^{-\frac{E_j - E_i}{kT}} = \frac{A_{0m} g_m}{A_{0n} g_n} e^{-\frac{\Delta E}{kT}} \quad (8)$$

For the same or similar crystal structure of different compounds, $\frac{A_{0m} g_m}{A_{0n} g_n}$ is quite approximate, when the temperature is same,

$$\frac{I_m}{I_n} \propto e^{-\Delta E} \quad (9)$$

Therefore, we conclude that the higher activation energy ΔE is, the better thermal stabilities is. However, it is only limited to the same or similar crystal structure of different compounds. As is mentioned above, these three compounds share the quite similar crystal structure, the thermal stabilities of $K_{0.2}Rb_{0.8}Ba_{0.97}PO_4$:$0.03Eu^{2+}$ is the best among these three compounds, and its activation energy is also the highest one, as shown in **Fig. 7** and **Fig. 8**.

The high thermal stability for the $K_{0.2}Rb_{0.8}Ba_{0.97}PO_4$:$0.03Eu^{2+}$ sample in the

present series can be also described by the neighboring-cation effect.[32] As shown in **Fig. 9**, the distances bewteen Eu^{2+} activator ions and the neighbor cations are originated from the previous Rietveld results, where the distance of Eu-K in $KBa_{0.97}PO_4$: Eu^{2+} is 3.856 Å which is smaller than the distance of Eu-Rb in $RbBa_{0.97}PO_4$: Eu^{2+} 3.962Å. The smaller distance can increase the larger Coulombic force following the Inverse-square law[33-34], resulting in the decrease in the thermal quenching barrier height, then the thermal stabilities become lower. Furthermore, we found that the distances of Eu-K in $K_{0.2}Rb_{0.8}Ba_{0.97}PO_4$:$Eu^{2+}$ turned into 3.952Å, which is longer than 3.856Å in $KBa_{0.97}PO_4$: Eu^{2+}, and the distance of Eu-Rb became 3.938Å, which is shorter than 3.962Å in $RbBa_{0.97}PO_4$: Eu^{2+}. The bond length variation in Eu-K (from 3.856 to 3.952 Å) is 4 times than that in Eu-Rb (from 3.962 to 3.938 Å), the huge change in Eu-K should make a great contribution to the difference of the thermal stabilities.

Fig. 10 presents the room temperature PL decay curves of $KBa_{0.97}PO_4$:$0.03Eu^{2+}$, $RbBa_{0.97}PO_4$:$0.03Eu^{2+}$ and $K_{0.2}Rb_{0.8}Ba_{0.97}PO_4$:$0.03Eu^{2+}$ samples, the decay curves can be fitted well by the follow equation: [35]

$$I(t) = I_0 + A\exp(-\frac{t}{\tau}) \qquad (10)$$

where I and I_0 are the luminescence intensity at time t and 0, A is a constant, t is the time, and τ is the lifetime. We obtained the lifetime values of $KBa_{0.97}PO_4$:$0.03Eu^{2+}$, $RbBa_{0.97}PO_4$:$0.03Eu^{2+}$ and $K_{0.2}Rb_{0.8}Ba_{0.97}PO_4$:$0.03Eu^{2+}$ which were 538.73 ns, 552.35ns and 484.04 ns, respectively. We can find that the three samples perform similar lifetimes which can prove further that they share the same crystal structure

except for some small difference among the cell parameters. The CIE chromaticity diagram and the corresponding positions for the typical phosphors, $K_{0.2}Rb_{0.8}Ba_{0.97}PO_4$:0.03$Eu^{2+}$, the commercially available $BaMgAl_{10}O_{17}$:Eu^{2+}, $KBa_{0.97}PO_4$:0.03Eu^{2+} and $RbBa_{0.97}PO_4$:0.03Eu^{2+}, were given in **Fig. 11**, and the inset also shows the digital phosphor photos under 365 nm UV-lamp excitation. It is found that all the phosphors can show intense blue emission, which indicates that this series of phosphors can find application in the white light-emitting diodes as the blue component.

4. Conclusions

In summary, a series of blue-emitting (K,Rb)$BaPO_4$:Eu^{2+} phosphors have been prepared. The continuous iso-structural solid-solution phases have been determined base on the Rietveld refinement. $K_xRb_{1-x}Ba_{1-0.97}PO_4$:0.03$Eu^{2+}$ (x=0-1) solid-solution phosphors exhibit the intense blue-emitting color with emission peak in the range of 410–430 nm, and the emission peaks shifted towards the long wavelength region with increasing Rb contents. The K/Rb ratio dependent luminescence behaviors have been also discussed based on the *d*-orbital splitting induced by the structural evolution. The thermal stable luminescence properties have been discussed in detail, and the relationship between the practical thermal stabilities and the calculated activation energy ΔE is discussed. It is found that $K_{0.2}Rb_{0.8}Ba_{0.97}PO_4$:0.03$Eu^{2+}$ phosphor shows the best thermal stability with the largest activation energy ΔE of 93.68%. The present findings indicates that the composition optimized (K_x,Rb_{1-x})$BaPO_4$:Eu^{2+} phosphor can be potential in the application of the phosphor-converted *w*-LEDs.

ACKNOWLEDGMENTS

The present work was supported by the National Natural Science Foundations of China (Grant No. No.51002146, No.51272242), Natural Science Foundations of Beijing (2132050), the Program for New Century Excellent Talents in University of Ministry of Education of China (NCET-12-0950), Beijing Nova Program (Z131103000413047), Beijing Youth Excellent Talent Program (YETP0635) and the Funds of the State Key Laboratory of New Ceramics and Fine Processing, Tsinghua University (KF201306). Z. G. Xia also thanks for the financial support from University of Science and Technology Beijing.

References

[1] W. Wanmaker and H. Spier, *J. Electrochem. Soc.*, 1962, **109**, 109.

[2] M. Ben Amara, M. Vlasse, G. Le Flem and P. Hagenmuller, *Acta Crystallogr.* , 1983, **39**, 1483.

[3] R. Masse and A. Dufif, *J. Solid State Chem.*, 1987, **71**, 574.

[4] Z. C. Wu, J. X. Shi, M. L. Gong, J. Wang and Q. Su, *Mater. Chem. Phys.*, 2007, **103**, 415.

[5] J. Y. Sun, X. Y. Zhang, Z. G. Xia and H. Y. Du, *J. Appl. Phys.*, 2012, **111**, 013101.

[6] Z. Wu, J. Liu, M. Gong and Q. Su, *J. Electrochem. Soc.*, 2009, **156,** 153.

[7] W. J. Tang and D. H. Chen, *J. Am. Ceram. Soc*., 2009, **92**, 1059.

[8] C. C. Lin and R.-S. Liu, *J. Phys. Chem. Lett.*, 2011, **2**, 1268.

[9] A. A. Setlur, W. J. Heward, Y. Gao, A. M. Srivastava, R. G. Chandran and M. V. Shankar, *Chem. Mater.*, 2006, **18**, 3314.

[10] M. M. Shang, G. G. Li, X. J. Kang, D. M. Yang, D. L. Geng and J. Lin, *ACS Appl. Mater. Interfaces*, 2011, **3**, 2738.

[11] T. Nishida, T. Ban and N Kobayashi, *Appl. Phys. Lett*. 2003, **82**, 3817.

[12] M. Y. Peng and L. Wondraczek, *Opt. Lett.* 2010, **35**, 2544.

[13] R. J. Xie, N. Hirosaki, K. Sakuma, Y. Yamamoto and M. Mitomo, *Appl. Phys. Lett.*, 2004, **84**, 5404.

[14] R. Masse and A. Durif, *J. Solid State Chem.*, 1987, **71**, 574.

[15] W. B. Im, H. S. Yoo, S. Vaidyanathan, K. H. Kwon, H. J. Park, Y. I. Kim and D. Y. Jeon, *Mater. Chem. Phys.*, 2009, **115,** 161.

[16] H. J. Song, D. K. Yim, H. S. Roh, I. S. Cho, S. J. Kim, Y. H. Jin, H. W. Shim, D. W. Kim and K. S. Hong, *J. Mater. Chem. C.*, 2013, **1**, 500-505.

[17] L. El Ammari and B. Elouadi, J. *Alloys Compd*, 1992, **188**, 99.

[18] A.C. Larson and R.B. Von Dreele, *Los Alos National Laboratory Report LAUR.* , 1994, **86**, 748.

[19] B. H. Toby, *J. Appl. Cryst.*, 2001, **34**, 210.

[20] A. R. Denton and N. W. Ashcroft, *Phys. Rev. A.*, **1991, 43,** 3161.

[21] L. G. Van Uitert, *J. Lumin*., 1984, **29**, 1.

[22] Z. G. Xia, J. Y. Sun, H. Y. Du and W. Zhou, *Opt. Mater*., 2006, 28, 524.

[24] L. G. Van Uitert, *J. Electrochem. Soc.*, 1967, **114**, 1048.

[23] L. Ozawa and P. M. Jaffe., *J. Electrochem. Soc.* 1971, **118**, 1678.

[25] G. Blasse, *Phys. Lett. A*., 1969, **28**, 444.

[26] G. Blasse, *J. Solid State Chem.*, 1986, **62**, 207.

[27] P. D. Rack and P. H. Holloway, *Mater. Sci. Eng. B*., 1998, **21**, 171.

[28] W. B. Im. N. F. Natalie, S. P. DenBaars, R. Seshadri and Young-Il, *Chem. Mater.*, 2009, **21**, 2957.

[29] J. Lu, F. P. Du, R. Zhu, Y. L. Huang and H. J. Seo, *J. Mater. Chem.*, 2011, **21**, 16398.

[30] S. Ye, J. H. Zhang, X. Zhang, S. Z. Lu, X. G. Ren and X. J. Wang, *J. Appl. Phys.*, 2007, **101**, 063545.

[31] S.Y. Zhang, Y. Nakai, T. Tsuboi, Y Zhang and H. J. Seo, *Inorg. Chem.*, 2011, **50,** 2897.

[32] W. Y. Huang, F. Yoshimure, K. Ueda, Y. Shimomura, H. S. Sheu, T. S. Chen, H. F. Greer, W. Z. Zhou. S. F. Hu, R. S. Liu and J. P. Attfield, *J. Am. Chem. Soc.*, 2012, **134**, 14108.

[33] C. A. Coulomb, "Premier mémoire sur l'électricité et le magnétisme". *Histoire de l'Académie Royale des Sciences. Imprimerie Royale*. 1785, pp. 569–577.

[34] D. J. Griffiths, Introduction to Electrodynamics (3rd ed.). *Prentice Hall*. 1998, ISBN 0-13-805326-X.

[35] Z. G. Xia, X. M. Wang, Y. X. Wang, L. B. Liao and X. P. Jing, *Inorg. Chem.*, **2011**, *50*, 10134.

Tables and figures captions are as follows,

Table 1. Main crystallographic parameters for $KBaPO_4$:0.03Eu^{2+}, $RbBaPO_4$:0.03Eu^{2+} and $K_{0.2}Rb_{0.8}BaPO_4$:0.03Eu^{2+} from the GSAS Program Rietveld Refinement

Fig. 1. XRD patterns of the a) $RbBa_{0.97}PO_4$:0.03Eu^{2+}, b) $K_{0.2}Rb_{0.8}Ba_{0.97}PO_4$:0.03$Eu^{2+}$, and c) $KBa_{0.97}PO_4$:0.03Eu^{2+} phosphors and the standard patterns of JCPDS-81-647 and JCPDS-84-1462.

Fig. 2. Powder XRD patterns for Rietveld structure analysis of the selected a) $KBaPO_4$:0.03Eu^{2+}, b) $RbBaPO_4$:0.03Eu^{2+}, c) $K_{0.2}Rb_{0.8}BaPO_4$:0.03Eu^{2+} based on the $KBaPO_4$ phase model and d) $K_{0.2}Rb_{0.8}BaPO_4$:0.03Eu^{2+} based on the $RbBaPO_4$ phase model.

Fig. 3. Lattice constants *a*, *b*, *c* and unit cell volume *V* of $K_xRb_{1-x}Ba_{0.97}PO_4$: 0.03Eu^{2+} solid-solution are plotted in a), b), c) and d).

Fig. 4. PLE and PL spectra of as-prepared $K_{0.2}Rb_{0.8}Ba_{0.97}PO_4$:0.03$Eu^{2+}$ phosphor.

Fig. 5. PL spectra of the $K_xRb_{1-x}Ba_{1-0.97}PO_4$:0.03$Eu^{2+}$ solid-solution phosphor with various K/Rb ratios.

Fig. 6. The red shift of peak wavelength for a) $KBa_{1-x}PO_4$:*x*Eu^{2+}, b) $K_{0.2}Rb_{0.8}Ba_{1-x}PO_4$:*x*$Eu^{2+}$ and c) $RbBa_{1-x}PO_4$:*x*Eu^{2+} phosphors with various Eu^{2+} concentrations.

Fig. 7. Temperature dependence of the PL spectra of a) $KBa_{0.97}PO_4$:0.03Eu^{2+}, b) $RbBa_{0.97}PO_4$:0.03Eu^{2+} and c) $K_{0.2}Rb_{0.8}Ba_{0.97}PO_4$:0.03$Eu^{2+}$ phosphors and the inset shows the relative intensity as a function of the temperature of the phosphor.

Fig. 8. The Arrhenius fitting of the emission intensity of a) $KBa_{0.97}PO_4$:0.03Eu^{2+}, b)

$KBa_{0.97}PO_4$:0.03Eu^{2+} and c) $K_{0.2}Rb_{0.8}Ba_{0.97}PO_4$:0.03$Eu^{2+}$ phosphors and the activation energy (ΔE) for the thermal quenching.

Fig. 9. The distances bewteen Eu^{2+} activator ions and the neighbor cations for a) $KBa_{0.97}PO_4$: Eu^{2+}, b) $KBa_{0.97}PO_4$: Eu^{2+} and c) $K_{0.2}Rb_{0.8}Ba_{0.97}PO_4$: Eu^{2+}, and the bond length values are obtained from the Rietveld results.

Fig. 10. Room temperature decay curves of $KBa_{0.97}PO_4$:0.03Eu^{2+} (red curve), $RbBa_{0.97}PO_4$:0.03Eu^{2+} (black curve) and $K_{0.2}Rb_{0.8}Ba_{0.97}PO_4$:0.03$Eu^{2+}$ (cyan curve) phosphors.

Fig. 11. CIE chromaticity diagram and the selected phosphor images, and the inset shows the positions of a) $K_{0.2}Rb_{0.8}Ba_{0.97}PO_4$:0.03$Eu^{2+}$, b) the commercially available $BaMgAl_{10}O_{17}$:Eu^{2+}, c) $KBa_{0.97}PO_4$:0.03Eu^{2+} and d) $RbBa_{0.97}PO_4$:0.03Eu^{2+} phosphors under 365 nm UV-lamp excitation.

Table 1. Main crystallographic parameters for $KBaPO_4$:0.03Eu^{2+}, $RbBaPO_4$:0.03Eu^{2+} and $K_{0.2}Rb_{0.8}BaPO_4$:0.03Eu^{2+} from the GSAS program Rietveld Refinement

Formula	**$KBaPO_4$: 0.03Eu^{2+}**	**$RbBaPO_4$: 0.03Eu^{2+}**	**$K_{0.2}Rb_{0.8}BaPO_4$: 0.03Eu^{2+}**	
Origin code	ICSD-202430	ICSD-72001	ICSD-202430	ICSD-72001
crystal system	orthorhombic			
space group	*P n m a (62)*			
$\alpha = \beta = \gamma$, º	90			
2θ-interval, º	5-120			
***a* (Å)**	7.714(8)	7.804(5)	7.747(6)	7.747(1)
***b* (Å)**	5.659(6)	5.728(5)	5.692(5)	5.691(7)
***c* (Å)**	9.965(1)	10.039(7)	9.991(5)	9.892(0)
***V* (Å^3)**	435.107	448.862	440.668	440.542
Z	4			
R_{wp}(%)	4.91%	2.67%	4.79%	4.06%
R_p(%)	2.26%	1.69%	2.43%	2.33%

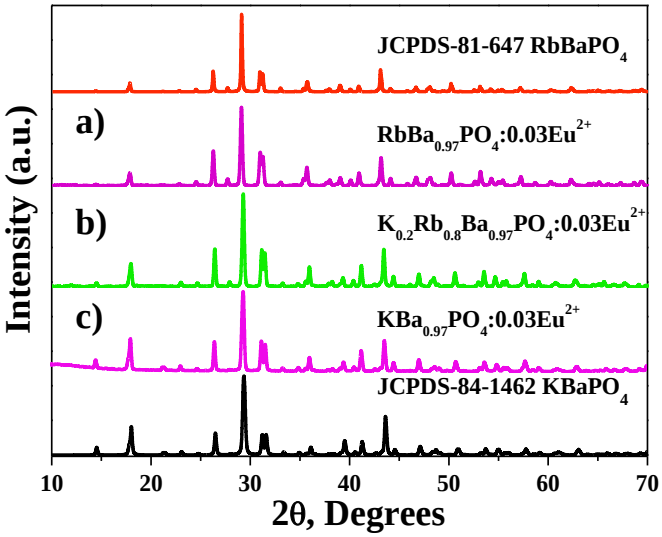

Fig. 1. XRD patterns of the a) $RbBa_{0.97}PO_4:0.03Eu^{2+}$, b) $K_{0.2}Rb_{0.8}Ba_{0.97}PO_4:0.03Eu^{2+}$, and c) $KBa_{0.97}PO_4:0.03Eu^{2+}$ phosphors and the standard patterns of JCPDS-81-647 and JCPDS-84-1462.

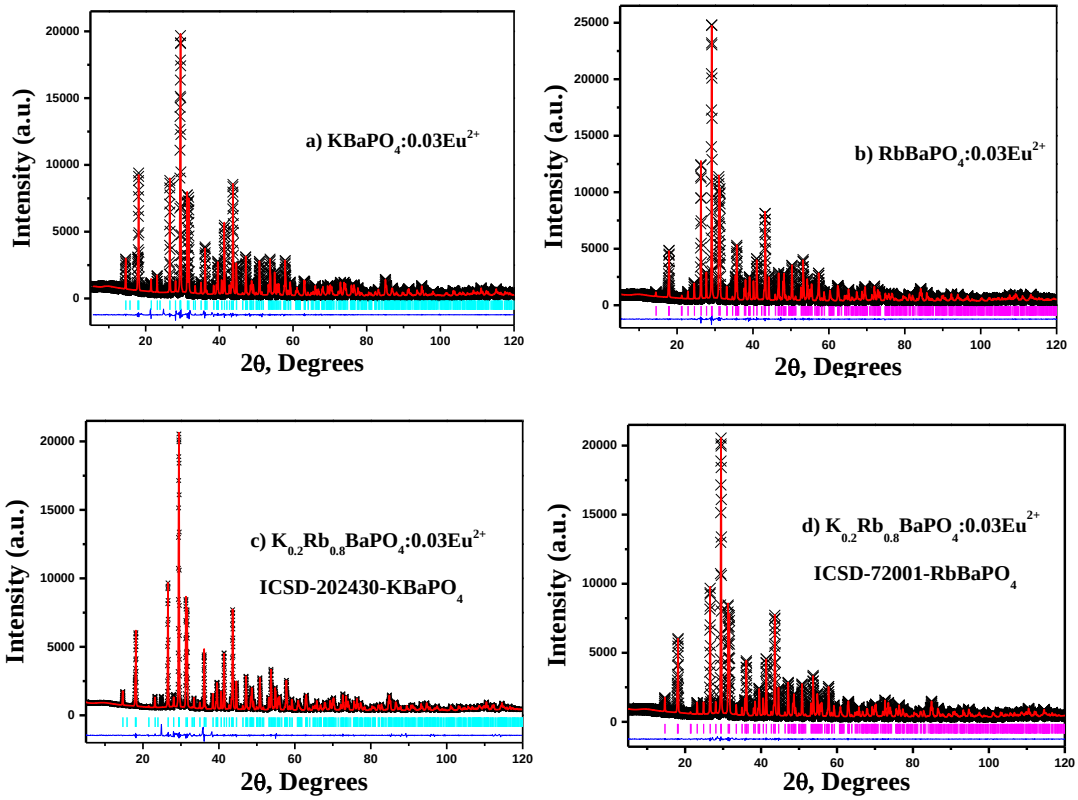

Fig. 2. Powder XRD patterns for Rietveld structure analysis of the selected a) $KBaPO_4$:0.03Eu^{2+}, b) $RbBaPO_4$:0.03Eu^{2+}, c) $K_{0.2}Rb_{0.8}BaPO_4$:0.03Eu^{2+} based on the $KBaPO_4$ phase model and d) $K_{0.2}Rb_{0.8}BaPO_4$:0.03Eu^{2+} based on the $RbBaPO_4$ phase model.

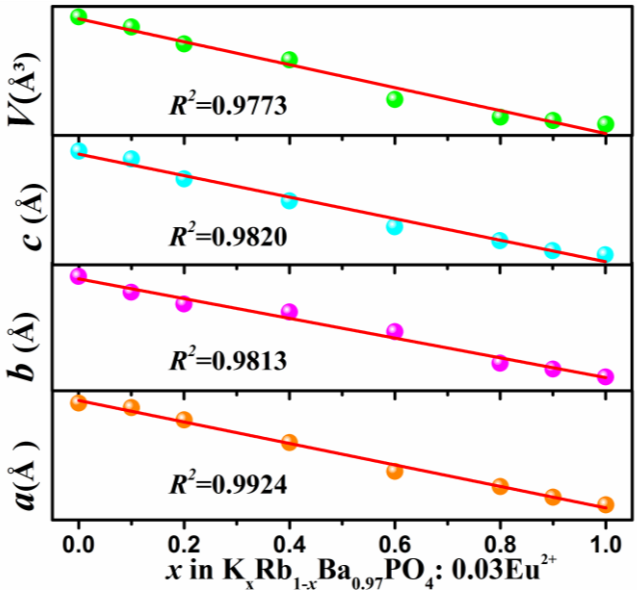

Fig. 3. Lattice constants *a*, *b*, *c* and unit cell volume *V* of $K_xRb_{1-x}Ba_{0.97}PO_4$: $0.03Eu^{2+}$ solid-solution are plotted in a), b), c) and d).

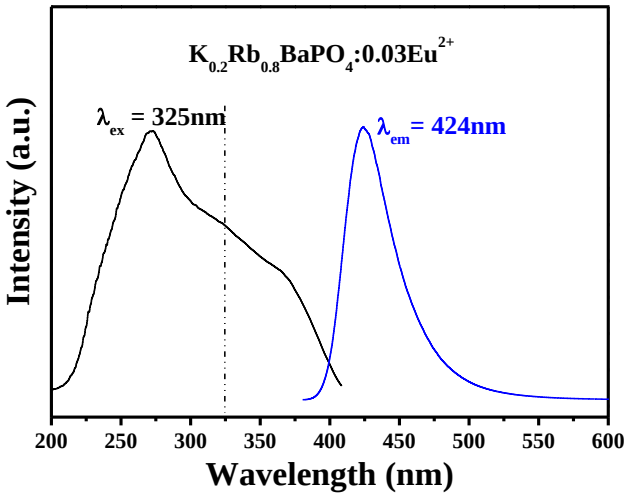

Fig. 4. PLE and PL spectra of as-prepared $K_{0.2}Rb_{0.8}Ba_{0.97}PO_4:0.03Eu^{2+}$ phosphor.

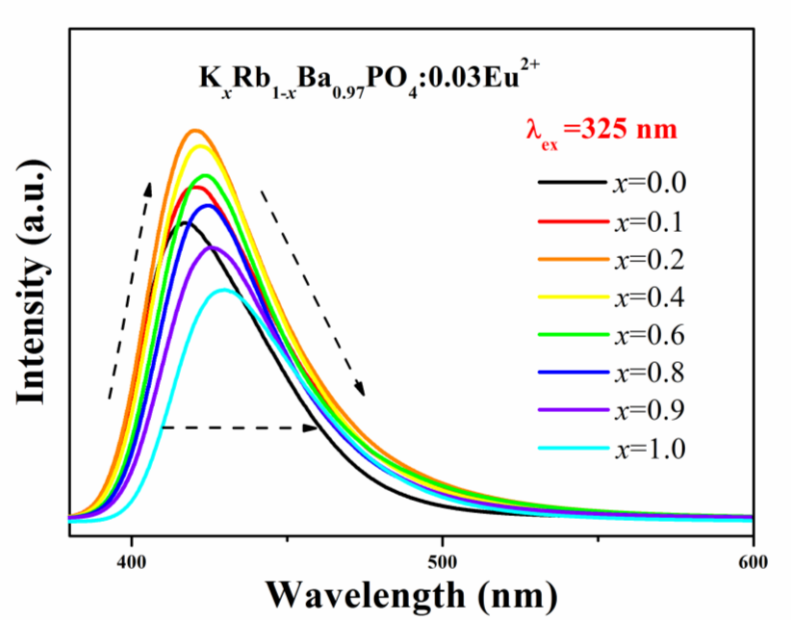

Fig. 5. PL spectra of the $K_xRb_{1-x}Ba_{1-0.97}PO_4:0.03Eu^{2+}$ solid-solution phosphor with various K/Rb ratios.

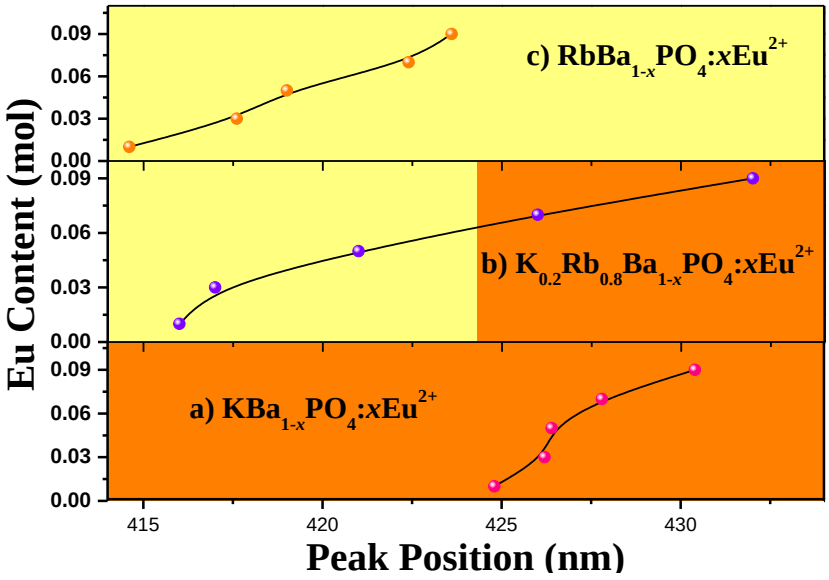

Fig. 6. The red shift of peak wavelength for a) $KBa_{1-x}PO_4:xEu^{2+}$, b) $K_{0.2}Rb_{0.8}Ba_{1-x}PO_4:xEu^{2+}$ and c) $RbBa_{1-x}PO_4:xEu^{2+}$ phosphors with various Eu^{2+} concentrations.

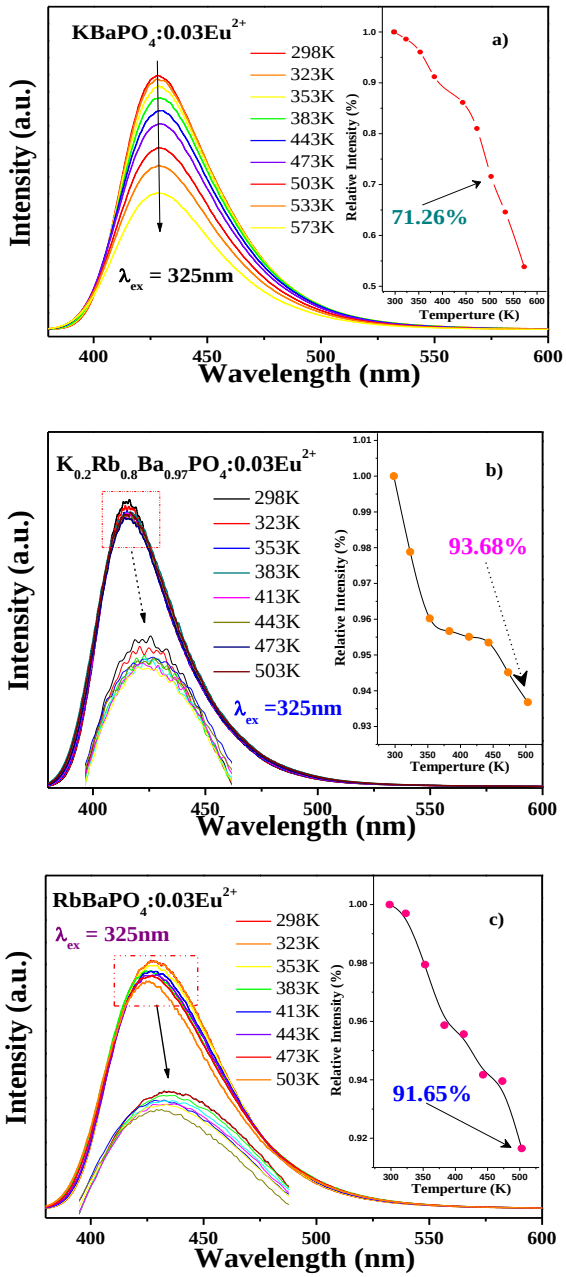

Fig. 7. Temperature dependence of the PL spectra of a) $KBa_{0.97}PO_4:0.03Eu^{2+}$, b) $K_{0.2}Rb_{0.8}Ba_{0.97}PO_4:0.03Eu^{2+}$ and c) $RbBa_{0.97}PO_4:0.03Eu^{2+}$ phosphors and the inset shows the relative intensity as a function of the temperature of the phosphor.

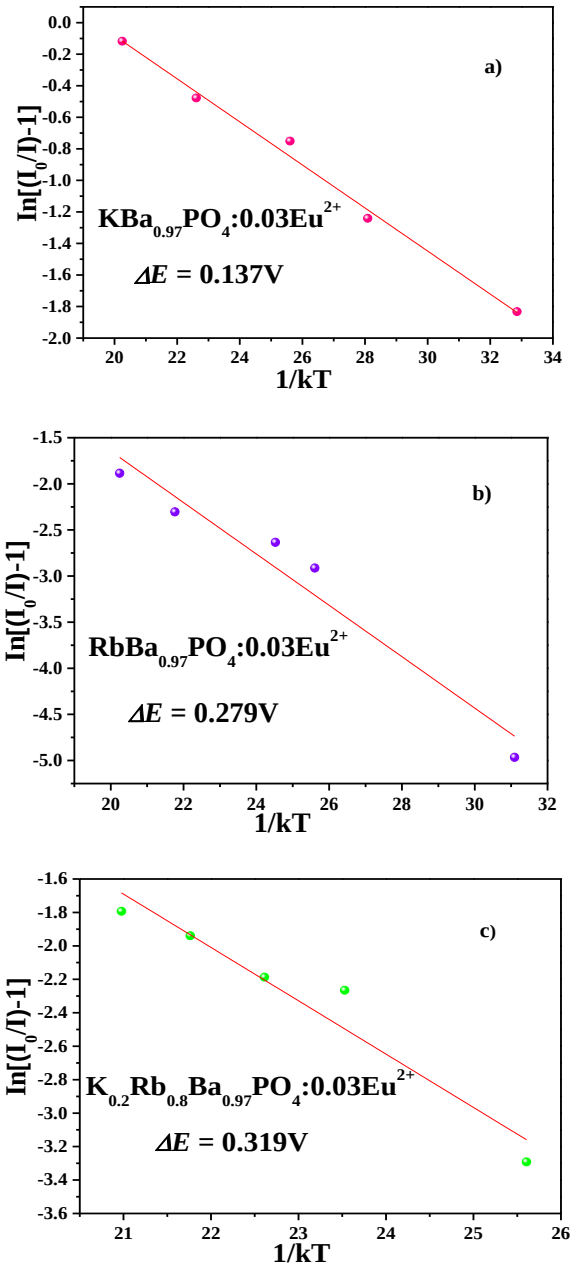

Fig. 8. The Arrhenius fitting of the emission intensity of a) $KBa_{0.97}PO_4:0.03Eu^{2+}$, b) $KBa_{0.97}PO_4:0.03Eu^{2+}$ and c) $K_{0.2}Rb_{0.8}Ba_{0.97}PO_4:0.03Eu^{2+}$ phosphors and the activation energy (ΔE) for the thermal quenching.

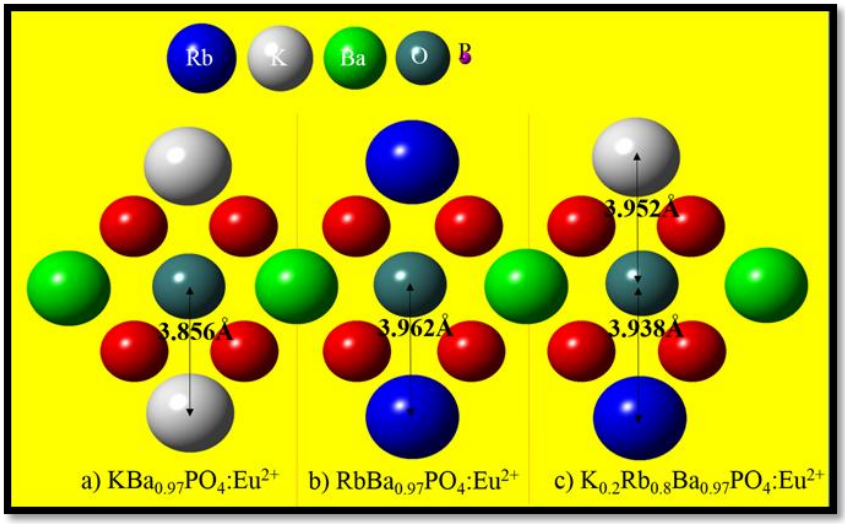

Fig. 9. The distances bewteen Eu^{2+} activator ions and the neighbor cations for a) $KBa_{0.97}PO_4$: Eu^{2+}, b) $KBa_{0.97}PO_4$: Eu^{2+} and c) $K_{0.2}Rb_{0.8}Ba_{0.97}PO_4$: Eu^{2+}, and the bond length values are obtained from the Rietveld results.

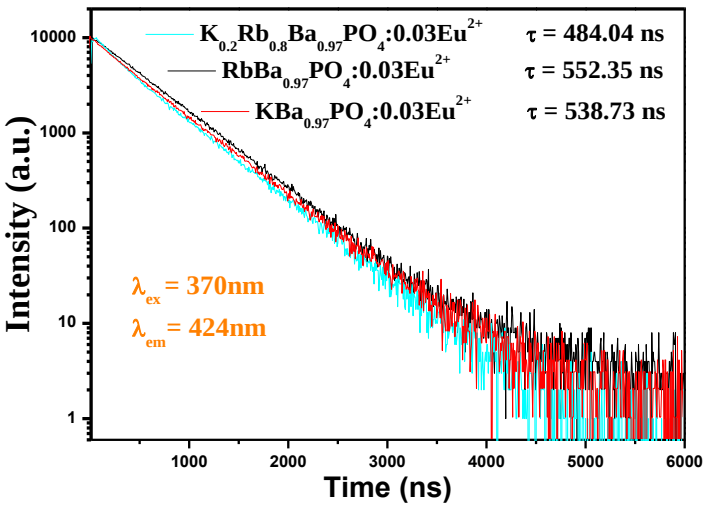

Fig. 10. Room temperature decay curves of $KBa_{0.97}PO_4$:0.03Eu^{2+} (red curve), $RbBa_{0.97}PO_4$:0.03Eu^{2+} (black curve) and $K_{0.2}Rb_{0.8}Ba_{0.97}PO_4$:0.03Eu^{2+} (cyan curve) phosphors.

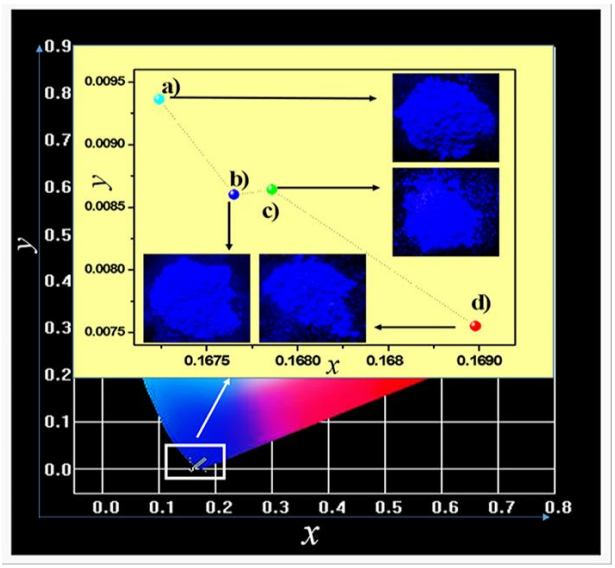

Fig. 11. CIE chromaticity diagram and the selected phosphor images, and the inset shows the positions of a) $K_{0.2}Rb_{0.8}Ba_{0.97}PO_4$:0.03$Eu^{2+}$, b) the commercially available $BaMgAl_{10}O_{17}$:Eu^{2+}, c) $KBa_{0.97}PO_4$:0.03Eu^{2+} and d) $RbBa_{0.97}PO_4$:0.03Eu^{2+} phosphors under 365 nm UV-lamp excitation.

Thermal Stable Luminescence and Structure Evolution of (K,Rb)$BaPO_4$:Eu^{2+} Solid-Solution Phosphors

Chenglong Zhao[1], Zhiguo Xia[2*], Shixin Yu[1]

[1]*School of Materials Sciences and Technology, China University of Geosciences, Beijing 100083, China*

[2]*School of Materials Sciences and Engineering, University of Science and Technology Beijing, Beijing 100083, China*

Thermal stable luminescence and structure evolution of the orthophosphate phosphors $ABaPO_4$:Eu^{2+} (A = K, Rb) were discussed.